



RESEARCH ARTICLE

Turbulence Around Auroral Arcs

10.1029/2023JA032309

Key Points:

- Small-scale auroral plasma turbulence is created preferably outside of but not far from optical auroral forms
- Turbulence appears both poleward and equatorward of auroral arcs
- Strong electric fields that trigger meter-size E region turbulence are sometimes seen before the onset of optical aurora

Supporting Information:

Supporting Information may be found in the online version of this article.










Correspondence to:

M. F. Ivarsen,
m.f.ivarsen@fys.uio.no

Citation:

Ivarsen, M. F., Huyghebaert, D. R., Gillies, M. D., St-Maurice, J.-P., Themens, D. R., Oppenheim, M., et al. (2024). Turbulence around auroral arcs. *Journal of Geophysical Research: Space Physics*, 129, e2023JA032309. <https://doi.org/10.1029/2023JA032309>

Received 22 NOV 2023
 Accepted 28 JUL 2024

Magnus F. Ivarsen^{1,2} , Devin R. Huyghebaert^{2,3} , Megan D. Gillies^{4,5} , Jean-Pierre St-Maurice^{2,6} , David R. Themens^{7,8} , Meers Oppenheim⁹ , Björn J. Gustavsson³ , Daniel Billett², Brian Pitzel² , Draven Galeschuk², Eric Donovan⁴, and Glenn C. Hussey² 

¹Department of Physics, University of Oslo, Oslo, Norway, ²Department of Physics and Engineering Physics, University of Saskatchewan, Saskatoon, SK, Canada, ³Department of Physics and Technology, UiT The Arctic University of Norway, Tromsø, Norway, ⁴Department of Physics, University of Calgary, Calgary, AB, Canada, ⁵Now at Mount Royal University, Calgary, AB, Canada, ⁶Department of Physics and Astronomy, University of Western Ontario, London, ON, Canada, ⁷School of Engineering, University of Birmingham, Birmingham, UK, ⁸Department of Physics, University of New Brunswick, Fredericton, NB, Canada, ⁹Astronomy Department, Boston University, Boston, MA, USA

Abstract The spectacular visual displays from the aurora come from curtains of excited atoms and molecules, impacted by energetic charged particles. These particles are accelerated from great distances in Earth's magnetotail, causing them to precipitate into the ionosphere. Energetic particle precipitation is associated with currents that generate electric fields, and the end result is a dissipation of the hundreds of gigawatts to terrawatts of energy injected into Earth's atmosphere during geomagnetic storms. While much is known about how the aurora dissipates energy through Joule heating, little is known about how it does so via small-scale plasma *turbulence*. Here we show the first set of combined radar and optical images that track the position of this turbulence, relative to particle precipitation, with high spatial precision. During two geomagnetic storms occurring in 2021, we unambiguously show that small-scale turbulence (several meters) is preferentially created on the edges of auroral forms. We find that turbulence appears both poleward and equatorward of auroral forms, as well as being nestled between auroral forms in the north-south direction. These measurements make it clear that small scale auroral plasma turbulence is an integral part of the electrical current system created by the aurora, in the sense that turbulent transport around auroral forms enhances ionospheric energy deposition through Joule heating while at the same time reducing the average strength of the electric field.

Plain Language Summary The aurora continues to amaze the inhabitants and travelers of Earth's polar regions. Bright shifting folds of light extend down from the night sky, appearing as green, red, or faint-blue curtains. During geomagnetic storms they are particularly bright and dynamic, often visible in large parts of the inhabited globe. However, far from being simple displays of light, the aurora can wreak havoc on the thin gas of Earth's upper atmosphere. There, gigantic swirls of electric turbulence are excited in response to the energy that is being pumped into the atmosphere by the aurora. This plasma turbulence is detrimental to satellite communication, such as the principle operation of the GPS network, and future efforts are sorely needed to understand when and how this turbulence appears. We present a series of photographic and radar-based images of the aurora and its plasma turbulence, shedding light on the complex relationship between the two phenomena. The images and videos we present are accessible and interesting to a public readership.

1. Introduction

The aurora is a beautiful display of bright light in the sky, appearing intermittently at night in Earth's high latitude regions. It often resembles slowly moving curtains hanging down from above. Borovsky et al. offer a succinct explanation: “an auroral arc is a geomagnetic east-west aligned curtain of optical emission in the upper atmosphere produced by the impacts of magnetospheric electrons that were accelerated downward along Earth's magnetic field” (p. 2 Borovsky et al., 2019). Auroral arcs are immensely important to the study of Earth's space environment. They represent channels through which the magnetosphere can transfer large amounts of energy to the ionosphere (Borovsky et al., 2019; Lysak et al., 2020). The dissipation of this energy inside the ionosphere leads, in turn, to the proliferation of turbulence, also referred to as plasma irregularities (Huba et al., 1985). To make matters more complicated, turbulence changes conductivity locally, which duly influences far-flung magnetospheric plasma flows (Dimant & Oppenheim, 2011; Wiltberger et al., 2017).

©2024. The Author(s).

This is an open access article under the terms of the [Creative Commons Attribution License](https://creativecommons.org/licenses/by/4.0/), which permits use, distribution and reproduction in any medium, provided the original work is properly cited.

The aurora is frequently accompanied by small scale (meter-size) plasma turbulence in the bottom-side ionosphere (the E-region). This turbulence *scatters* radio waves, observations of which have given rise to the term “radar aurora” (Hysell, 2015), but these fluctuations in the plasma are also responsible for detrimental radio signal scintillations affecting satellite navigation (Kintner et al., 2007; Semeter et al., 2017; Yeh & Liu, 1982). The turbulence that causes the radar aurora is triggered by the Farley-Buneman (FB) instability, which results from the relative difference between ion and electron velocities, itself introduced by collisions between charged particles and neutral gas molecules (Buneman, 1963; Farley, 1963). If this relative drift is sufficiently large, meter-scale wave structures will grow perpendicular to Earth's magnetic field lines (Fejer & Kelley, 1980). These turbulent waves can impact the entire magnetosphere-ionosphere-thermosphere system through changes in the auroral conductivities (Dimant & Oppenheim, 2011; Liu et al., 2018; Oppenheim, 1997). Indeed, given strong electric fields, electron heating from turbulence can exceed classical Joule heating (St-Maurice & Goodwin, 2021). Electric fields in the ionosphere enable large-scale current systems, giving auroral plasma irregularities the moniker “electrojet turbulence” (Oppenheim, 1997; Senior et al., 1982). Much like storms in Earth's lower atmosphere influence the larger weather system, electrojet turbulence exerts a tangible effect on the entire geospace system (Wiltberger et al., 2017). Some studies predict that auroral turbulence is capable of doubling ionospheric conductivities locally (e.g., Dimant & Oppenheim, 2011), and so the configuration of the magnetosphere system must change in response.

Previous observations have pointed to a tendency for the radar aurora to occur outside the optical aurora (Bahcivan et al., 2006; Hall et al., 1990; Huyghebaert et al., 2021; Hysell et al., 2012). In the present report we present examples without ambiguities of a systematic connection between edges of the optical aurora and the radar aurora. This connection is particularly clear-cut for discrete auroral arcs, and it strongly supports the notion that plasma turbulence emerges preferably in the low-density regions outside high-energy electron precipitation. Here, currents are too weak to short out the electric field, owing to the reduced electrical conductivity that comes with reduced ionization. Specifically, many observations around quiescent auroral arcs have shown that the region just outside arcs exhibits enhanced electric fields (Karlsson et al., 2020).

The foregoing agrees with the notion that the basic origin of auroral arcs lies in roughly U-shaped quasi-static potential structures originating in the magnetosphere and mapping to the ionosphere during particle precipitation events (Mozer et al., 1977; Roth et al., 1993), and this scenario has been shown to be the case for discrete auroral arcs (Echim et al., 2009; Imajo et al., 2021). A simplified view is on display in panel a of Figure 1. The electric potential structures can also be the result of Alfvénic acceleration (Lysak & Song, 2003), a product of anomalous (turbulent) resistivity turning Alfvén waves into electrostatic structures (Lysak & Dum, 1983), or arise through Alfvén wave reflection events in the ionosphere (Mallinckrodt & Carlson, 1978). In principle, any beam of precipitating electrons from the magnetosphere should work like an electron gun shooting charged particles toward the ionosphere. In Figure 1, the beam of electrons (green slab) drives an electrical current (referred to as Birkeland currents), with a current flow upwards, opposite to that of the streaming electrons. Fanning out horizontally from the beam would be the Pedersen currents that close the current system together with *downward* Birkeland currents that form outside of the precipitation region (Marklund, 2009).

New parallel electric fields are created at ionospheric heights (Figure 1c), and this drives parallel return currents through thermal electrons. A current loop that involves the precipitating and thermal electrons is then set up. The precipitating electrons create an electric field perturbation in a direction perpendicular to the geomagnetic field, which in turn leads to currents that flow along the thus-created perpendicular electric field. The final part of the loop involves return currents carried by thermal electrons in the region that surrounds the region of precipitation. The precise region over which the return currents are distributed depends on long list of factors: the precipitating energy flux, the particle flux, the ambient electric field strength and direction, centers of symmetry for cylindrical precipitation patterns, the actual orientation of the precipitation band if the region is elongated, and the sharpness of the transition from precipitation to no-precipitation (Dahlgren et al., 2011; de Boer et al., 2010; Marklund, 2009; Noël et al., 2000, 2005; St. Maurice et al., 1996). While Hall currents are also present, they do not close current loops unless they are at certain unusual locations like the end points of finite length auroral arcs.

To complicate matters, the aforementioned currents dissipate magnetospheric energy locally through Joule heating (e.g., Thayer, 1998, and references therein), analogously to currents generating heat inside an incandescent lightbulb. Combined with strong electric fields, heating caused directly by auroral turbulence can constitute a significant part of the total Joule dissipation (St-Maurice & Goodwin, 2021). Additionally, in places

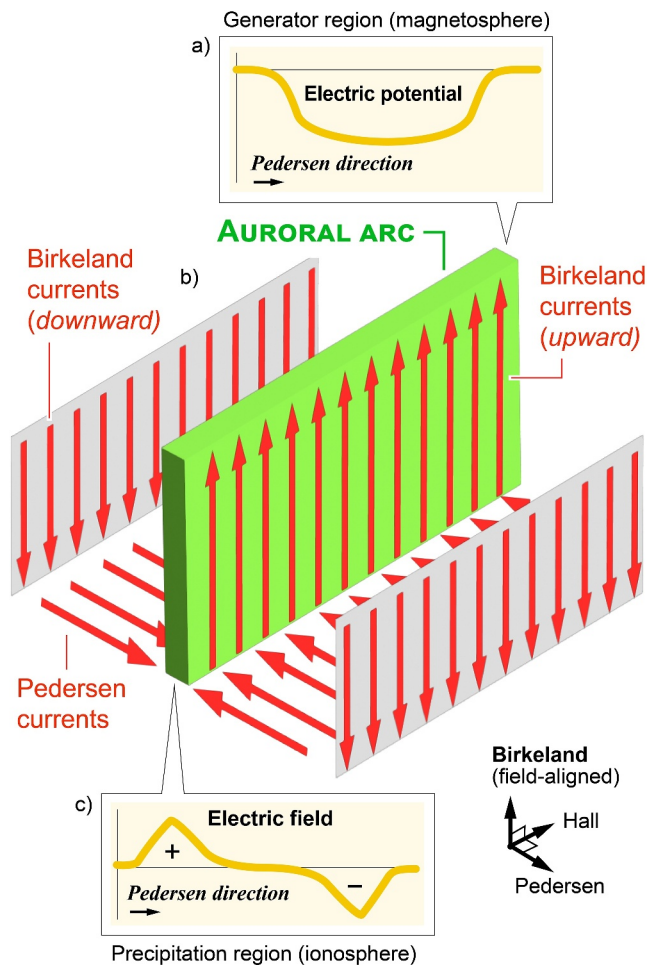


Figure 1. Diagram of the idealized current system surrounding an auroral arc (green central slab, panel b). The auroral arc is powered by an equipotential structure in the magnetospheric generator region (Borovsky et al., 2019; Lysak et al., 2020), shown in Panel (a). Downward precipitating electrons drive the upwards Birkeland currents, which close through the ionospheric E-region (Marklund, 2009). Panel (c) shows the ionospheric electric field around the arc in the E-region, which is enhanced on the edges of the arc (de Boer et al., 2010; Noël et al., 2005).

where there are thermal (electron) return currents, anomalous heating may dampen small-scale turbulent growth rates inside auroral arcs (Dimant et al., 2021).

In light of the above, it becomes crucial to understand where auroral turbulence emerges, as it provides vital information about the auroral electric field. In addition, anomalous conductivity, or turbulent resistivity, affects both conductances and overall dissipation rates, which in turn must be accounted for in order to accurately model space weather (Dimant & Oppenheim, 2011). Large-scale models deviate from nature during disturbed conditions (Siscoe et al., 2002; Winglee et al., 1997). At the same time, the E-region ionosphere is notoriously understudied. In fact, owing to the difficulty of observing the bottomside ionosphere, a recent review article describing the 80–200 km altitude region brought back the term “ignosphere” (Palmroth et al., 2021), to highlight the urgency with which auroral turbulence must be understood.

To put the above paragraphs in simplified terms, we evoke an observer in one of Earth's high latitude regions, looking up into the night sky. The focus becomes the observation of the bottomside ionosphere, namely the E-region, which acts as the surface of Earth's space plasma environment. Here, turbulent processes interact with the aurora, modifying key electrical properties that reverberate throughout Earth's magnetosphere. With the goal of shedding crucial light on these processes, we turn to the new experimental ICEBEAR radar. It is capable of imaging a collection of individual FB waves as a 3D point cloud. Through geomagnetic coordinate transformations we can turn this point cloud into a *mesh* that surrounds the spatial distribution of auroral turbulence (Ivarsen, Lozinsky, et al., 2023; Ivarsen, St-Maurice, Hussey, Spicher, et al., 2023).

As mentioned, previous studies have found a spatial offset between the radar and optical aurora (Bahcivan et al., 2006; Hall et al., 1990; Huyghebaert et al., 2021; Hysell et al., 2012). However, all previous studies were plagued by ambiguities and other limitations. The ambiguities included range aliasing in radar data (Bahcivan et al., 2006; Hysell et al., 2012), optical measurements near the horizon (Bahcivan et al., 2006), poor resolution in optical and radar measurements (Hall et al., 1990), and a dependency on strong detrimental refraction to see the radar aurora at all (Watermann, 1990). Crucially, all the previous studies were projecting the received radar power onto a *constant-altitude sky-surface*. In the auroral region, this projection must be done toward the horizon, where Earth's magnetic field lines are perpendicular to the

look direction. ICEBEAR's unique capability of imaging turbulent shapes through 3D point clouds clears up these ambiguities. With ICEBEAR, E-region radar hardware and signal processing techniques are now at a sufficiently advanced stage that we can begin to uncover many of the intricate physical processes on the bottomside of the ionosphere, a region that is notoriously difficult to measure.

2. Methods

The Ionospheric Continuous-wave E-region Bistatic Experimental Auroral Radar (ICEBEAR, operated by the University of Saskatchewan) is a 49.5 MHz coherent scatter radar located in Canada with a field-of-view (FOV) overlooking northern Saskatchewan (Huyghebaert et al., 2019). ICEBEAR consists of a transmitter near Prelate, SK (50.9°N, 109.4°W), and a receiver north-east of Saskatoon, SK (52.2°N, 106.5°W). It is operating with very low elevation angles, yielding aspect angles that are almost field-perpendicular. Using a coded pseudo random continuous-wave (CW) signal the radar is able to obtain simultaneous resolutions of 1.5 km and 1 s in range and time, respectively. The receiver consists of 10 antennas with unequal spacing to obtain unambiguous azimuthal and elevation details of the scattered signal (Lozinsky et al., 2022). The resolution in azimuth and elevation is $\sim 0.1^\circ$.

The radar range does not alias for 30,000 km due to the coding scheme used. This means that we expect zero occurrence of range errors due to aliasing—most data is within 2,000 km of the radar. We also use longer and more baselines in the analysis compared to previous studies (15 cross spectra for Hysell et al. (2012) vs. 45 for ICEBEAR). As alluded to in the Introduction, E-region coherent scatter radar echoes are predominantly caused by unstable FB waves, and ICEBEAR's operating frequency means that its signal will scatter off of 3-m density irregularities. As a result, the ICEBEAR 3D dataproduct consists of the full 3D spatial locations of individual FB echoes, along with their signal-to-noise ratio (SNR) and Doppler velocities. During particularly disturbed conditions, ICEBEAR can record more than 1,000 such individual FB waves per second.

Alongside radio echoes from auroral plasma turbulence we analyze observations of the aurora itself. These are made using the multi-instrument Transition Region Explorer (TREX) RGB Imager, a true-color auroral imaging system operated by the University of Calgary (Gillies et al., 2019, 2020). The primary optical instrument is based on the state-of-the-art Canon ME20F-SH high-sensitivity detector, a 35 mm CMOS sensor specially designed to produce a low-light color balance identical to that of human perception (Gillies et al., 2020; Kikuchi et al., 2016). The sensor is housed in an all-sky-imager instrument, which is a fish-eye lens mounted on a digital camera pointing straight up, capable of a 360° view. The system is shutter-less, and can operate with a 100% duty cycle to provide a continuous video feed. The feed is in turn partitioned into frames that each cover 3 s of observations (a composite image based on nine 1/3 s exposures in sequence). Each frame is a 558 × 480 pixel true-color image; the spatial location of CCD pixels are then transformed into the Altitude-adjusted Corrected Geomagnetic Coordinate system (Baker & Wing, 1989), following the procedure outlined in Gillies et al. (2020), and assuming an overall emission altitude of 110 km. The result is a 558 × 480 grid of geomagnetic coordinates, to which the true-color image can be *mapped*. The TREX system used in the present study is located at the Rabbit Lake research site in Saskatchewan, Canada (58.22°N, 103.68°W), situated near the middle of ICEBEAR's field-of-view.

The analysis performed in the present paper will be presented in the form of commentaries to conjugate radar- and optical observations, and no specialized mathematical or statistical methods are applied to the data, other than those described in the present Section 2. As such, the analysis is accessible to workers of various stripes in the field of space physics.

Figure 2 provides a complete overview of the observational platforms we rely on, and the geometric considerations of combining the ground-based systems. First, panel a shows the high-latitude ionosphere, plotted by magnetic longitude and magnetic latitude. The region highlighted with a red rectangle is where ICEBEAR 3D's field-of-view closely overlaps with the Rabbit Lake research station's magnetic zenith (where the TREX RGB system is looking parallel to Earth's magnetic field lines). This region in MLON-MLAT space is considered more closely in panels b–d. In panel b we show in black contour lines the theoretical aspect angles of the ICEBEAR 3D echoes observed from an altitude of 105 km (the overall median ICEBEAR 3D backscatter altitude; Ivarsen, St-Maurice, Hussey, Galeschuk, et al., 2023), using the International Geomagnetic Reference Field to estimate geomagnetic field vectors. The geomagnetic location of Rabbit Lake (its field-aligned zenith) is indicated with a yellow cross. In panel c we display with a gray color scale the radar gain pattern, where we average across all altitudes. In panel d we show in black contour lines the average nearest-neighbor distance between the TREX RGB pixel centers, after the image is mapped to geomagnetic coordinates. The two red- and blue-colored rectangles in Figures 2b and 2c show the MLON-MLAT extent of the three events analyzed in the present study. Here, we see that theoretical aspect angles are appreciably small (<1°) and optical image resolution appreciably high (pixel size <4 km).

Within the altitudinal extent we consider, there is uncertainty associated with the precise altitude from which auroral emissions originate. However, from the assumptions laid out so far and the intensity of the optical green-line emissions, particle precipitation in the lower E-region is expected. Since Earth's magnetic field lines are nearly vertical at these latitudes (inclination angles are here usually lower than 15°), any variation between 95 and 115 km does not introduce significant changes in the horizontal (field-perpendicular) positions of the aurora. With these points in mind, we have been able to compare the location of the radar echoes with that of the optical aurora, as described in more detail in the Section 3.

Lastly in our treatment of the Methodology, we must address the issue of refraction. Density structures produced by the aurora might refract the reflected radio signal before it is received by the radar. This will lead to an offset between the true path of the signal and the apparent (observed) elevation angles of that signal. To shed light on the matter, we ran a ray-tracing algorithm. The ray-tracing simulations were conducted with the PHaRLAP (Cervera & Harris, 2014) ray-tracing package through an ionosphere simulated by the Empirical Canadian High Arctic

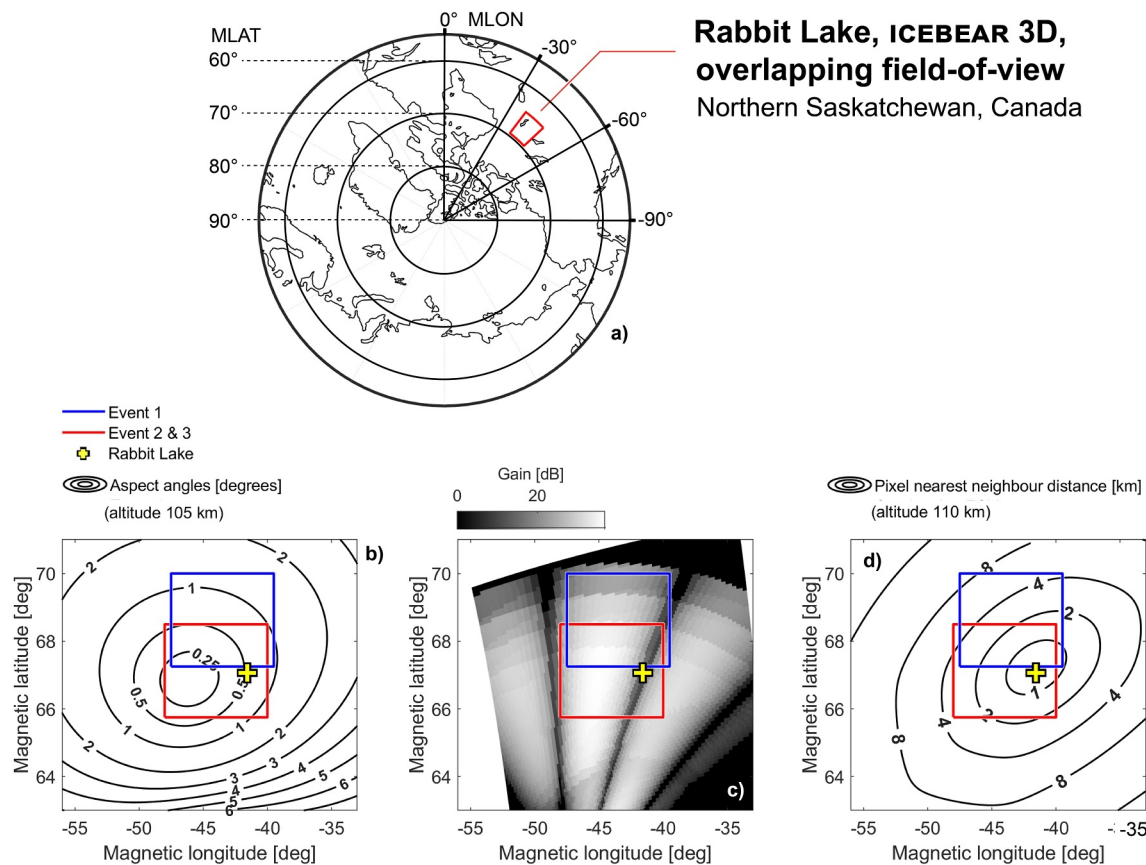


Figure 2. Panel (a): the location of the two instruments used in the present report: the ICEBEAR auroral radar and the TREX RGB auroral imager, plotted in geomagnetic coordinates, with Earth's coastlines indicated (this location's MLT lags UT by around 6.5 hr). Panel (b) shows contour lines of constant modeled aspect angles, using International Geomagnetic Reference Field for Earth's magnetic field. Panel (c) shows the radar power gain pattern with colorscale indicated. Panel (d) shows the nearest neighbor distance between adjacent TREX RGB pixels after mapping the image to geomagnetic coordinates. In Panels (b–d), the spatial boundaries for Figure 3 are shown in blue, and boundaries for Figures 4 and 5 are shown in red. The location of Rabbit Lake (magnetic zenith) is plotted with a yellow cross.

Ionospheric Model (Themens et al., 2017, 2018, 2019) with particle precipitation prescribed by its auroral E-Region option (Watson et al., 2021). To simulate a “worst-case” scenario, the simulation was run throughout the night of 7–8 September 2017, that is, during one of the largest geomagnetic storms of the last solar cycle. The results show that the worst case introduces a maximum spatial horizontal offset of 2 km inside the Rabbit Lake research station's zenith. With Figure 2 in mind, we conclude that the assumption of geomagnetic field-perpendicularity is achieved, and that the uncertainty in spatial locations due to refraction is much smaller than the effective TREX RGB pixel size in this region.

3. Results

We provide here three different examples of events with joint data from the ICEBEAR radar and the TREX RGB (True-Color) auroral imager, instruments that have overlapping fields-of-view over the Rabbit Lake research station in Saskatchewan, Canada. Whereas the first event takes place during relatively quiet conditions, the latter two occurred during storms in geospace. The events were selected for the coincidental nature of their measurements as well as for the relatively discrete nature of their auroral forms (in a companion paper, Ivarsen et al., 2024), we examine auroral turbulence seen during a pulsating aurora event. We were thus looking for auroral forms with clear precipitation boundaries in regions of strong emission intensity. We will first present images of a simple event with 18 s integration time (Figure 3), going down to the maximum resolution of 3 s for events recorded during particularly disturbed conditions (Figures 4 and 5). Along the bottom of those three Figures we show an ICEBEAR-derived Doppler-time-intensity plot of the auroral turbulence. “Doppler velocity” refers to the velocity of the reflected radar signal with respect to the receiver, which is a measure of the turbulent wave phase velocity,

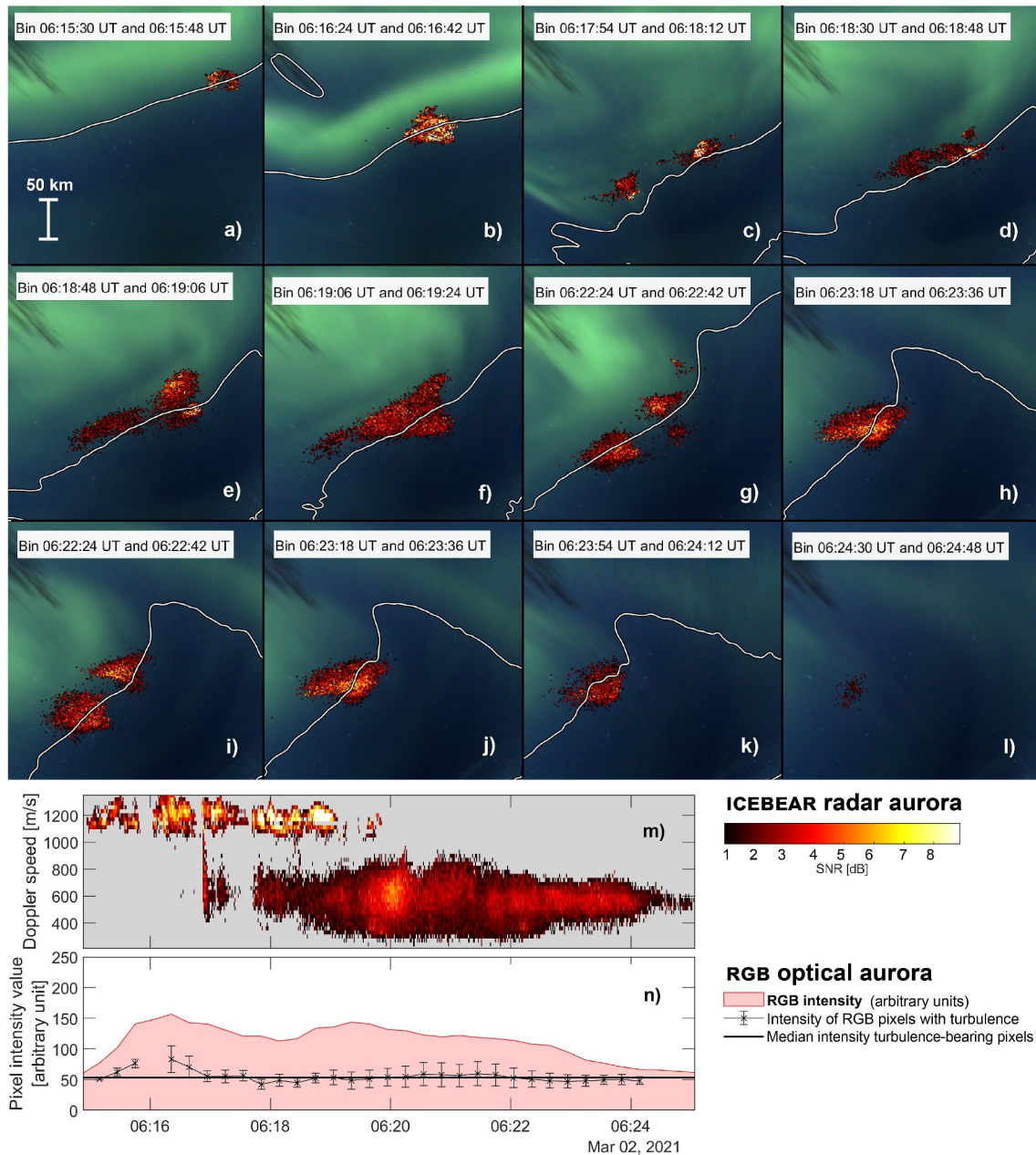


Figure 3. Spatial and temporal evolution of unstable plasma structures on the south-eastern edge of an auroral form. Panels (a–l): twelve 18 s snapshots of structures taken at irregular intervals between 06:15 UT and 06:25 UT on 2 March 2021, around local magnetic midnight. Each frame shows the distribution of ICEBEAR 3D measurements (color-coded by signal-to-noise ratio), superposed on RGB TREX auroral images mapped to geomagnetic coordinates (altitude 110 km). A single white line indicates a contour of constant auroral emission intensity that passes through the average position of all turbulent echo locations in a given panel. Panel (m) ICEBEAR Doppler-time-intensity diagram, with Doppler velocity (turbulent wave phase velocity) on the y-axis and SNR (turbulent wave spectral power) color coded. Panel (n): RGB TREX emission intensity, in the form of the 95th percentile value of all the pixels shown in each of the storyboard frames (pink shaded area). The average intensity of RGB pixels in locations where there is also ICEBEAR-measured radar aurora is plotted using black x-symbols with error-bars denoting standard deviation.

while intensity, or SNR, is a measure of turbulent wave spectral power against a noise background. Crucially, we include a plot showing TREX RGB auroral *emission intensity* (inside the region of interest), along with the mean intensity of RGB pixels in regions where plasma turbulence was present, a value that is strikingly consistent across all three events.

Figure 3 (and Movie S1) shows that ICEBEAR-measured radar aurora were present on the south-east side of the brightest auroral emissions measured by TREX RGB. The data were obtained on 2 March 2021, between 06:15 UT

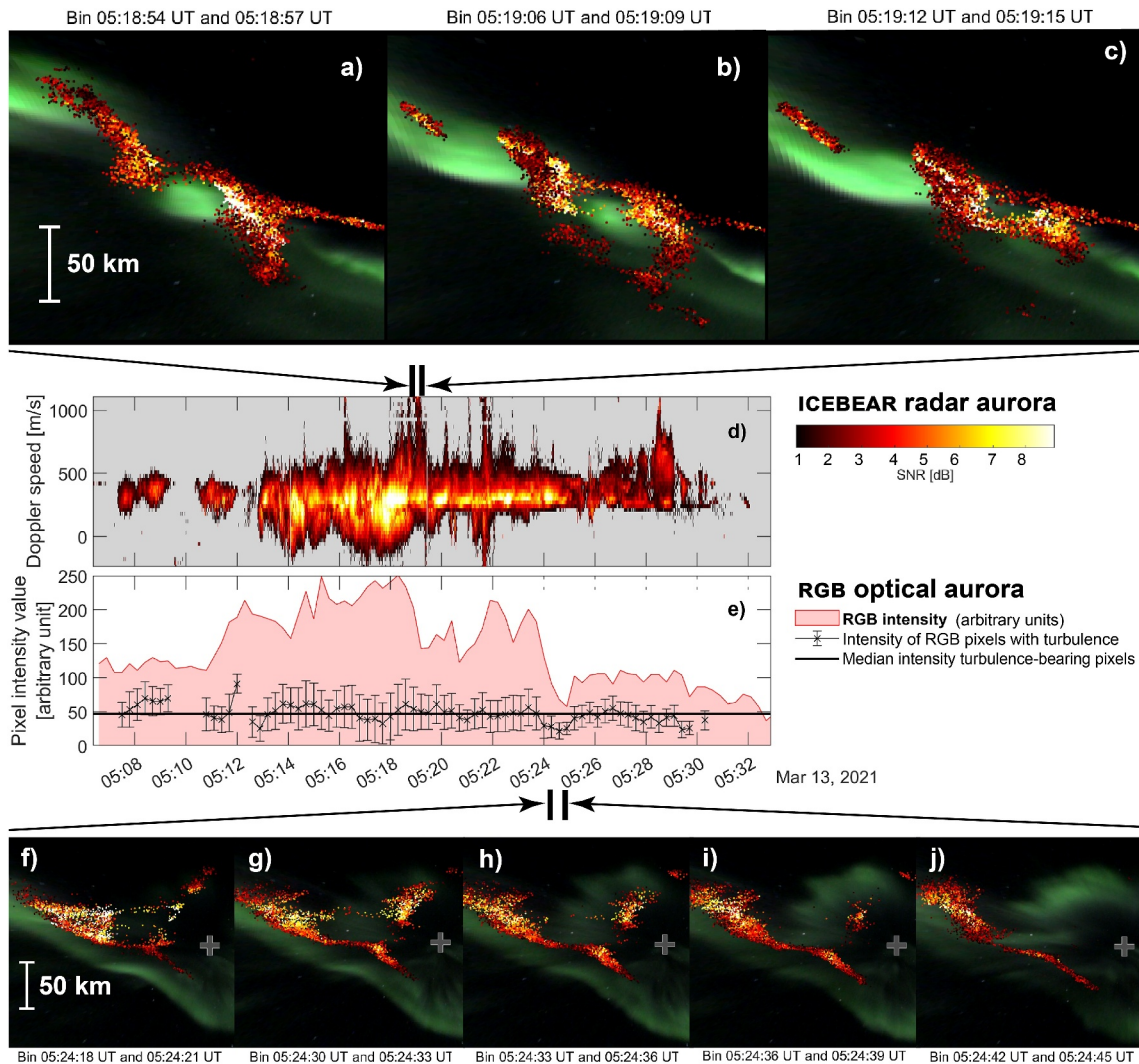


Figure 4. Same as in Figure 3 but for the spatial and temporal evolution of unstable plasma structures in and around one or more intense discrete arcs between 05:10 UT and 05:25 UT on 13 March 2021. Panels (a–c) show how turbulent regions wrap around the optical arcs during a short time span with spikes in the ICEBEAR radar aurora Doppler velocity (the turbulent wave phase velocity). Panels (f–j) detail how the radar aurora can act as a precursor to increased optical emissions.

and 06:25 UT. The radar scatter was initially populated by very fast Doppler shifts of the order of 1,200 m/s before transitioning to more typical FB turbulence speeds. The mixture of these fast and conventional modes indicates that the $E \times B$ drift velocity was equal to at least 1,200 m/s, and that plasma temperatures were enhanced owing to Joule and turbulent heating processes (St-Maurice et al., 2023).

Figure 3 reveals a particularly simple case of patches of unstable plasma turbulence appearing, and then disappearing, along the edge of a roughly east-west-oriented arc associated with a relatively diffuse aurora. Despite the diffuse character of the arc, there is a sharp gradient in the brightness intensity toward the arc. In panel j, the single white contour line passing through the average position of the turbulent regions is associated with a median emission intensity of 50 emission intensity units from the RGB TREX emissions averaged across the red, green, and blue channels. This is equal to 20% of the value which saturates the sensor, and it does not change much, even when the optical aurora itself flares up on two occasions (panels b and g in Figure 3).

Figure 4 provides a more dynamic example of conjugate radar and optical aurora measurements. Here we observe either one or two clear arc structures spanning the region of interest, oriented roughly in the east-west direction. As is clear from Movie S2 (and from Figure 4e), the observed turbulence aligns itself along an RGB-contour line of 50 emission intensity units, parallel to the optical arc. That the ICEBEAR radar aurora tends to occur at constant RGB

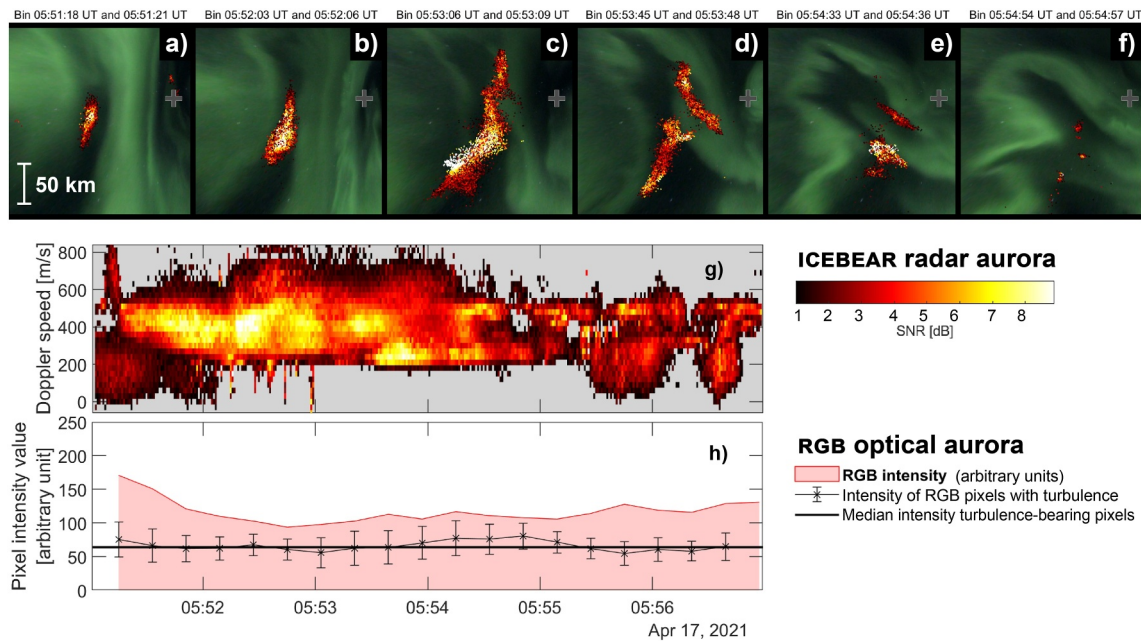


Figure 5. Same as Figure 3 but for the spatial and temporal evolution of an unstable plasma structure nestling between evolving auroral forms, occurring on 17 April 2021, between 05:51 UT and 05:55 UT, around local magnetic midnight.

intensity contour lines provides firm evidence that the mapping of optical data to geomagnetic coordinates together with ICEBEAR's spatial imaging algorithm ultimately succeed in drawing out the geometry of auroral turbulence with kilometer-precision.

Examples of conspicuous, disorderly and turbulent motion in both the optical and radar auroras occurs during the sudden increase in Doppler velocity spread in Figure 4e between 05:14 UT and 05:22 UT. Here, it is the aurora itself that breaks up, forming roughly circular patches. The turbulence then becomes particularly intense around those patches. This suggests that the arc geometry temporarily breaks into more cylindrical regions of precipitation, and is consistent with the notion of a perpendicular electric field that is still strong (very strong in fact) and not inside the region of precipitation, but rather in the region that surrounds it.

The prominent dip in the emission intensity favored by ICEBEAR that occurs around 05:25 UT (Figures 4f–4j) shows a clear, and relatively rare, example of a situation that is the reverse of the other observations thus far covered. Here, the optical emissions around the radar aurora in the upper right part of the panels (panel g in particular) are extremely weak while the radio echoes are very intense. We find a similar example being displayed in Figure 5 and Movie S3. Here, in addition to having north-south optical and radio echo patterns, we also see in Figure 5 an anomalous pattern that is becoming increasingly clear of strong radio echoes occurring when precipitation is weak, only to be followed by *weak* radio echoes when the optical aurora becomes far more intense. It should be clear that the FB echoes indicate the presence of a strong electric field. While an electrostatic interpretation for echoes parallel to long, well-defined auroral arcs was straightforward in terms of an electric field strength maximizing outside the precipitation region, we have here a challenge with very weak precipitation signatures (no large electron fluxes coming down) and yet a strong electric field sandwiched in between the two regions of very weak precipitation. This points to a non-electrostatic origin to the electric field, and this is particularly clear in Figure 5c. This in turn indicates the likelihood for an *electromagnetic* origin to the strong electric field, namely, the presence of an Alfvén wave at the particular location where the strong echoes are observed. This is entirely plausible since, during other events, we have indeed found strong radar echoes when satellite overpasses clearly indicated that an Alfvén wave was present overhead (not shown). If this interpretation is valid, then, it becomes interesting to see that the region of weak precipitation on each side of the radar echoes actually becomes stronger while at the very same time the SNR of the radio echoes becomes weaker and ultimately vanishes. Moreover, in the case of Figure 5, the optical emissions were stronger when the radio echoes were weaker *before* the radio echoes became stronger, indicating a cyclical phenomenon. This signifies that when

the Birkeland currents intensify, the resulting electrostatic electric field becomes too weak to produce strong radar echoes from FB turbulence (if any). Thus, at least for the examples found here, the electric field from an impinging Alfvén wave would have to be stronger than the electrostatic field that follows (or even precedes) the arrival of an Alfvén wave train.

In the Appendix A to the present paper, we present a technical analysis into the temporal anti-correlation between optical emissions and radio echoes at the same spatial location. The more technical representation in Figure A1 demonstrates that the radar aurora can, under some circumstances, directly *precede* the optical aurora.

As already eluded to above, the third event (Figure 5 and Movie S3) also differs from the first two in that both the optical emissions and radar aurora are oriented roughly along the north-south direction, extending over more than 100 km likely indicating that the aurora was “snaking around” on a larger scale covering the zonal direction. In this event, as a rule, it remains that the radar aurora is for the most part nestled inside a sharp crevice *between* the auroral forms. Initially, this turbulent structure grows greatly in bulk size and SNR, roughly following the auroral forms that constrict growth to a south-west-ward direction. Then the forms of the optical aurora evolve dynamically and intrude on the space previously occupied by the radar aurora.

4. Discussion

Our high resolution optical and radio observations unambiguously demonstrate that, as a rule, meter-size turbulence consistently occurs outside the brightest emission regions. This is true both of sharp discrete arcs (Figure 4) and of more diffuse forms (Figures 3 and 5). Across all events there is a strong tendency for the signature of turbulence, the radar aurora, to occur within a narrow range of auroral emission intensity (around 20% of the emission value that saturates the RGB sensor). The turbulent regions are on both sides of auroral arcs, as well as nestled between forms that extend in the north-south direction.

Which sides of auroral forms turbulence appears is dictated by where the ionospheric electric field is elevated. For arcs generated by U-shaped potential structures (such as in Figure 1), we expect to see auroral turbulence on both sides of the auroral arc. When we observe turbulence only on one side of the arc, it is likely that the ambient electric field (and the direction it is pointing in) cancels out the increase on the other side. This will effectively correspond to so-called “S-shaped” electric potentials (Marklund et al., 2007). The interaction between ambient drifts and the electric field created by an arc may well account for the variety of radar aurora configurations seen in the three events under consideration.

The auroral turbulence measured by ICEBEAR (turbulent FB waves that move in the Hall direction but can be observed from any direction) corresponds to regions of elevated electric fields, which drive currents. We thereby see the extent and orientation of the strongest Pedersen (and Hall) current regions. These regions map directly to the magnetospheric electric- and magnetic field modulations that powers the aurora through wave-particle interactions (Kasahara et al., 2018).

The coupling between field-aligned (or Birkeland) current and the strong electric field near precipitating regions begs the question: are the beams of precipitating electrons responsible for the perpendicular electric fields seen in the ionosphere, or is there a preexisting electric field that precipitating electrons are actually trying to short out? This is related to the age-old question: is the magnetosphere acting as a voltage source or a current source? It would appear that, for most of the time, the strong perpendicular electric fields responsible for FB turbulence are detected once there is a clear auroral form nearby, thereby pointing to a current generator. However, panels f–j of Figures 4 and 5, as well as Figure A1 in the Appendix, demonstrate that on occasions the radio echoes can be stronger when the optical aurora is weaker. We have suggested an electromagnetic source for such exceptions, namely, the electric field from a passing Alfvén wave train. Another electrostatic possibility would be that a voltage source is at least occasionally present instead of a current source. The question has added relevance in light of a recent discovery that the field-aligned current structuring (auroral filamentation) and E-region turbulence exhibit matching turbulent signatures at times (Ivarsen, Lozinsky, et al., 2023). Such filamentation in the aurora in turn contains a high Poynting flux and transfers Alfvénic energy (Billett et al., 2021; Keiling et al., 2019; Seyler et al., 1998). In a companion paper, we explore this topic further (Ivarsen et al., 2024).

To illustrate the effect of the aurora on the ionospheric current system when Birkeland currents and associated electrostatic fields are in control, we reproduce a frame from the second event. Figure 6a shows the radar aurora surrounding the edges of a discrete auroral arc that underwent a short interruption in space, thereby breaking the

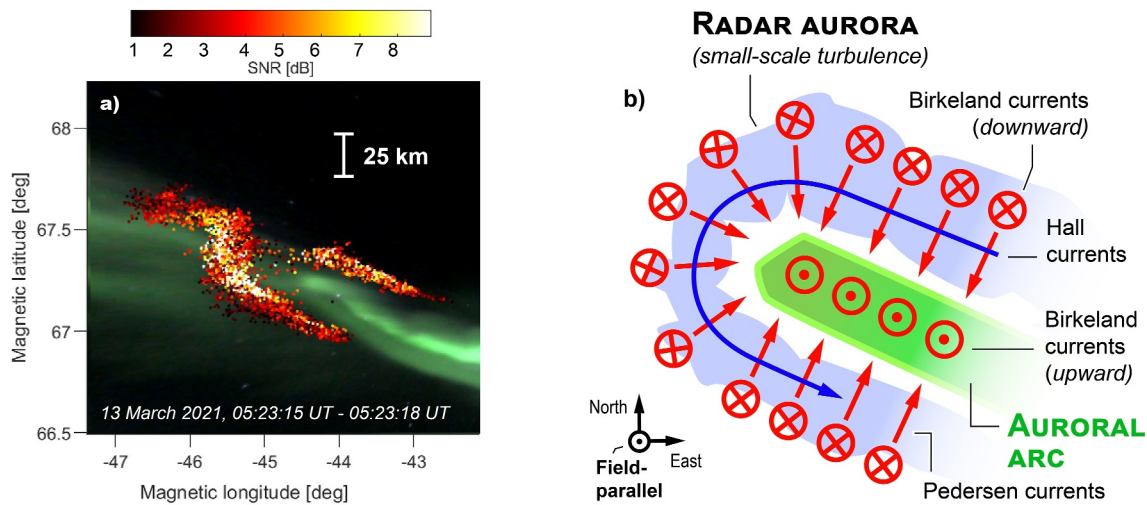


Figure 6. Coincident observations of the optical and radar aurora (panel a), and an idealized diagram of the subsequent auroral current system (panel b).

original into two arcs. In Figure 6b, we draw a diagram of the arc, based on the geometric model presented in the Introduction. Remarkably, there is a palpable resemblance between direct spatial observations and the idealized auroral current system on scales smaller than 25 km. The implications are clear. When we observe small-scale turbulence around auroral arcs, any thermal return current inside that arc would not help to close the current system, owing to the intense precipitating particle energy flux (de Boer et al., 2010). As argued in the Introduction, a build-up in electric field strength may then occur outside the auroral arc, to the point of causing widespread FB wave turbulence there. This, in turn, can increase energy dissipation rates systemwide (Schlegel & St.-Maurice, 1981; St.-Maurice & Goodwin, 2021).

Nominally, the radar signal Doppler velocity (a measure of the turbulent wave phase velocity) should allow us to determine the Hall current direction (blue arrow in Figure 6b). This being stated, the task is not as easily performed: the only sure thing about the Doppler shift of the fully turbulent modes (this excludes narrow spectral signatures associated with weak turbulence) is that they are largest along the relative ion-electron drift direction, which unfortunately rotates with altitude. In addition a vector reconstruction depends on assumptions about the connection between the threshold speed (nominally the ion-acoustic speed) and the angle between the wave-vector and the relative drift direction (Hysell, 2015).

As stated in the Introduction, refraction might play a small role in the localization of the unstable waves. The most unstable modes are created at very small aspect angles (a fraction of a degree) owing to the fact that they are described by kinetic solutions, rather than fluid solutions at a few m (St-Maurice et al., 2023). However, as stated in the Section 2, a worst-case scenario from our ray-tracing calculations indicates an uncertainty in ICEBEAR turbulent locations due to refraction that is smaller than typical TREX RGB pixel sizes.

5. Conclusion

Using state-of-the-art 3D radar data of auroral plasma turbulence from ICEBEAR in conjunction with the new TREX RGB True-color imager system, we have investigated the spatial locations of the radar aurora and those of optical auroral forms. The striking fidelity of our new radar data demonstrated, clearly and unambiguously, that the radar aurora skirts regions of bright optical auroral emission intensity, a feat that has eluded previous efforts due to measurement ambiguities.

The three-dimensional radar measurements presented here attest to the extraordinary temporal and spatial resolution of ICEBEAR. With kilometer-precision, the observations exhibit occasional rapidly shifting shapes of turbulent plasma—all following the outline of dancing auroral forms. These turbulent shapes inspire, in the mind of the writer and hopefully also in that of the reader, enquiries about the electric field distributions at the origin of the radar aurora. The ICEBEAR radar aurora is in a unique position to shed light on the ionosphere's E-region, which is not as accessible as the F region ionosphere since it cannot be accessed by satellites. This leaves radars as a tool of

choice. Incoherent scatter radars are not abundant as they are costly to build and operate. Coherent radars like ICEBEAR are far more accessible in terms of costs. They are limited to viewing large amplitude structures perpendicular to the magnetic field produced by turbulence. The more information we can extract from such radars, the better. Multi-link interferometry is adding a new wealth of information and showing the way forward.

The addition of detailed optical auroral information adds a key element to the coherent radar data. To wit: our new observations provide a link between the auroral current system that ultimately drives the optical aurora through accelerated particles and the electric fields that surrounds these areas of energetic particle precipitation. Mapping out this electric field remains a challenge in space physics, and the phenomena we describe involve several processes that affect how the electric field is modified or even *produced* by the aurora. Further observations of how the ionospheric electric field behaves will aid large-scale modeling experiments, the results of which currently deviate from nature during disturbed conditions (Siscoe et al., 2002; Winglee et al., 1997). In the future, the extraordinary fidelity with which ICEBEAR can image turbulent phenomena in space plasmas will inspire broad enquiries into exactly how storms in geospace lead to bursts of enormous energy dissipation in Earth's atmosphere, much of which is readily observed with the naked eye.

A final aspect worth mentioning relates to the fact that the strong electric fields that lead to FB turbulence are, at times, highly localized. While the auroral features are often highly dynamical and complicated, we have uncovered situations where strong electric fields are clearly limited to regions near the edge of auroral arcs. According to Noël et al. (2000, 2005) and de Boer et al. (2010), this localization should coincide with bursts of thermal electron downward currents overlapping the enhanced electric field regions. These bursts can be intense enough to produce strong electron heating if the edge of precipitation regions are sharp and the ambient electric field is strong. When coupled with ion frictional heating in the same regions, the hot electrons should drive regions of strongly enhanced ionospheric outflows. While there are at this time no other observations to support our claim—noting that the ICEBEAR radar and RGB optical observations are clear, explicit and numerous—it remains that the present findings are opening new research avenues that may be of great importance for a holistic understanding of geospace (Borovsky & Valdivia, 2018). This would be true not just for the study of turbulence and the role it plays, but also for what it may reveal about the nature of the electric fields that drive it.

Appendix A: Technical Analysis of the Radar Aurora Preceding Optical Emissions

The observation, and claim, that the radar aurora can precede optical emissions rather than being caused by them is, to our knowledge, novel and requires careful documentation. In addition to Figures 4 and 5, we therefore present in this appendix a detailed technical representation of this phenomenon.

At the location indicated by a red arrow in Figure A1, a clearly distinguished arc-like feature develop in the ICEBEAR echoes, starting from around 08:31:10 UT. This miniature arc-like feature reaches a maximum extent at around 08:31:19 UT, after which it starts to dissipate. By 08:31:31 UT a similarly shaped arc-like emission structure is forming just eastward of the diminishing echoes. By 08:31:37 UT a clear, and very intense, emission region has replaced the arc-like echo structure. By this time, the whole echo structure seem to have condensed into a arc-like feature that exists a few kilometers poleward of the distinct emission structure. By 08:31:46 UT the two miniature structures are seemingly dissipating in tandem, with the emissions moving westward to merge with the larger, more stable, emission region to the west of the theater. At 08:31:49 UT the original arc-like structure is indistinguishable, and the echoes have attached themselves to the larger westward emission region.

This remarkable event, which takes place in its entirety during some 30 s, demonstrates the complex relationship between the ionospheric electric field and auroral emissions, and serves as additional documentation for the claims and discussions presented in the Sections 3 and 4 of the present paper.

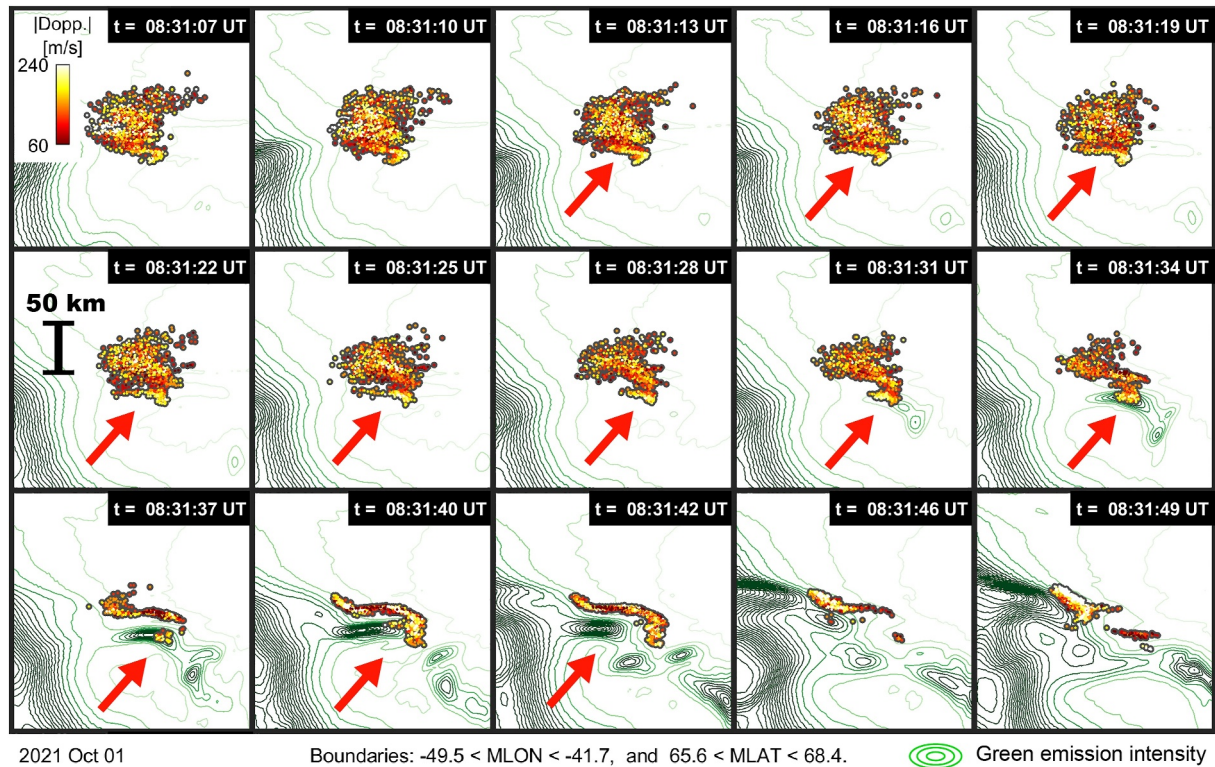


Figure A1. Detailed spatio-temporal evolution of a radar aurora echo cluster positioned outside of an intense and dynamic auroral form observed at 08:31 UT on 1 October 2021. Echo Doppler speed is indicated with a colorscale, while the auroral emission intensity is now shown by green contour lines of varying color, with the faintest emissions having a color close to white. A red arrow points to a particular spatial location in which the radar aurora forms along a small arc-like shape that becomes a prominent emission region some 10 seconds after the excitation of FB turbulence. In all 15 panels, the time of observation is posted in a black rectangle.

Data Availability Statement

ICEBEAR 3D echo data for 2020, 2021 is published with DOI <https://doi.org/10.5281/zenodo.7509022> (Hussey & Ivarsen, 2023). TRES optical data can be accessed at <https://data.phys.ucalgary.ca/> (RGB, 2023). E-CHAIM can be accessed at <http://e-chaim.chain-project.net/> PHaRLAP can be accessed at <https://www.dst.defence.gov.au/our-technologies/pharlap-provision-high-frequency-raytracing-laboratory-propagation-studies>.

Acknowledgments

This work is supported in part by Research Council of Norway (RCN) Grant 324859. We acknowledge the support of the Canadian Space Agency (CSA) (20SUGOICEB), the Canada Foundation for Innovation (CFI) John R. Evans Leaders Fund (32117), the Natural Science and Engineering Research Council (NSERC), the International Space Mission Training Program supported by the Collaborative Research and Training Experience (CREATE) (479771-2016), the Discovery grants program (RGPIN-2019-19135); and the Digital Research Alliance of Canada (RRG-FT2109). DRT acknowledges United Kingdom Natural Environment Research Council (NERC) EISCAT3D: Fine-scale structuring, scintillation, and electrodynamic (FINESSE) (NE/W003147/1) and DRivers and Impacts of Ionospheric Variability with EISCAT-3D (DRIIVE) (NE/W003368/1) projects. DRH acknowledges a UiT contribution to the EISCAT_3D project funded by RCN Grant 245683. MFI is grateful to I Ivarsen for language assistance.

References

- Bahcivan, H., Hysell, D. L., Lummerzheim, D., Larsen, M. F., & Pfaff, R. F. (2006). Observations of colocated optical and radar aurora. *Journal of Geophysical Research*, *111*(A12), A12308. <https://doi.org/10.1029/2006JA011923>
- Baker, K. B., & Wing, S. (1989). A new magnetic coordinate system for conjugate studies at high latitudes. *Journal of Geophysical Research*, *94*(A7), 9139–9143. <https://doi.org/10.1029/JA094iA07p09139>
- Billett, D. D., Perry, G. W., Clausen, L. B. N., Archer, W. E., McWilliams, K. A., Haaland, S., et al. (2021). The relationship between large scale thermospheric density enhancements and the spatial distribution of poyniting flux. *Journal of Geophysical Research: Space Physics*, *126*(5), e2021JA029205. <https://doi.org/10.1029/2021JA029205>
- Borovsky, J. E., Birn, J., Echim, M. M., Fujita, S., Lysak, R. L., Knudsen, D. J., et al. (2019). Quiescent discrete auroral arcs: A review of magnetospheric generator mechanisms. *Space Science Reviews*, *216*(1), 1. <https://doi.org/10.1007/s11214-019-0619-5>
- Borovsky, J. E., & Valdivia, J. A. (2018). The Earth's magnetosphere: A systems science overview and assessment. *Surveys in Geophysics*, *39*(5), 817–859. <https://doi.org/10.1007/s10712-018-9487-x>
- Buneman, O. (1963). Excitation of field aligned sound waves by electron streams. *Physical Review Letters*, *10*(7), 285–287. <https://doi.org/10.1103/PhysRevLett.10.285>
- Cervera, M. A., & Harris, T. J. (2014). Modeling ionospheric disturbance features in quasi-vertically incident ionograms using 3-D magnetoionic ray tracing and atmospheric gravity waves. *Journal of Geophysical Research: Space Physics*, *119*(1), 431–440. <https://doi.org/10.1002/2013JA019247>
- Dahlgren, H., Gustavsson, B., Lanchester, B. S., Ivchenko, N., Brändström, U., Whiter, D. K., et al. (2011). Energy and flux variations across thin auroral arcs. *Annales Geophysicae*, *29*(10), 1699–1712. <https://doi.org/10.5194/angeo-29-1699-2011>
- de Boer, J. D., Noël, J.-M. A., & St. Maurice, J.-P. (2010). The effects of mesoscale regions of precipitation on the ionospheric dynamics, electrodynamic and electron density in the presence of strong ambient electric fields. *Annales Geophysicae*, *28*(6), 1345–1360. <https://doi.org/10.5194/angeo-28-1345-2010>

- Dimant, Y. S., Khazanov, G. V., & Oppenheim, M. M. (2021). Effects of electron precipitation on E-region instabilities: Theoretical analysis. *Journal of Geophysical Research: Space Physics*, *126*(12), e2021JA029884. <https://doi.org/10.1029/2021JA029884>
- Dimant, Y. S., & Oppenheim, M. M. (2011). Magnetosphere-ionosphere coupling through E region turbulence: 2. Anomalous conductivities and frictional heating. *Journal of Geophysical Research*, *116*(A9), A09304. <https://doi.org/10.1029/2011JA016649>
- Echim, M. M., Maggiolo, R., Roth, M., & De Keyser, J. (2009). A magnetospheric generator driving ion and electron acceleration and electric currents in a discrete auroral arc observed by Cluster and DMSP. *Geophysical Research Letters*, *36*(12), L12111. <https://doi.org/10.1029/2009GL038343>
- Farley, D. T. (1963). A plasma instability resulting in field-aligned irregularities in the ionosphere. *Journal of Geophysical Research*, *68*(22), 6083–6097. <https://doi.org/10.1029/JZ068i022p06083>
- Fejer, B. G., & Kelley, M. C. (1980). Ionospheric irregularities. *Reviews of Geophysics*, *18*(2), 401–454. <https://doi.org/10.1029/RG018i002p0401>
- Gillies, D. M., Donovan, E., Hampton, D., Liang, J., Connors, M., Nishimura, Y., et al. (2019). First observations from the TReX spectrograph: The optical spectrum of STEVE and the picket fence phenomena. *Geophysical Research Letters*, *46*(13), 7207–7213. <https://doi.org/10.1029/2019GL083272>
- Gillies, D. M., Liang, J., Donovan, E., & Spanswick, E. (2020). The apparent motion of STEVE and the picket fence phenomena. *Geophysical Research Letters*, *47*(20), e2020GL088980. <https://doi.org/10.1029/2020GL088980>
- Hall, G., Moorcroft, D. R., Cogger, L. L., & Andre, D. (1990). Spatial relationship between large aspect angle VHF radio aurora and 557.7-nm emissions: Evidence for refraction. *Journal of Geophysical Research*, *95*(A9), 15281–15288. <https://doi.org/10.1029/JA095iA09p15281>
- Huba, J. D., Hassam, A. B., Schwartz, I. B., & Keskinen, M. J. (1985). Ionospheric turbulence: Interchange instabilities and chaotic fluid behavior. *Geophysical Research Letters*, *12*(1), 65–68. <https://doi.org/10.1029/GL012i001p00065>
- Hussey, G., & Ivarsen, M. (2023). ICEBEAR 3D coherent scatter radar data for 2020, 2021 (DATA). *Zenodo*. <https://doi.org/10.5281/zenodo.7509022>
- Huyghebaert, D., Hussey, G., Vierinen, J., McWilliams, K., & St-Maurice, J.-P. (2019). ICEBEAR: An all-digital bistatic coded continuous-wave radar for studies of the E region of the ionosphere. *Radio Science*, *54*(4), 349–364. <https://doi.org/10.1029/2018RS006747>
- Huyghebaert, D., St-Maurice, J.-P., McWilliams, K., Hussey, G., Howarth, A. D., Rutledge, P., & Erion, S. (2021). The properties of ICEBEAR E-region coherent radar echoes in the presence of near infrared auroral emissions, as measured by the swarm-E fast auroral imager. *Journal of Geophysical Research: Space Physics*, *126*(12), e2021JA029857. <https://doi.org/10.1029/2021JA029857>
- Hysell, D. L. (2015). The radar aurora. In *Auroral dynamics and space weather* (pp. 191–209). American Geophysical Union (AGU). <https://doi.org/10.1002/9781118978719.ch14>
- Hysell, D. L., Miceli, R., Munk, J., Hampton, D., Heinselman, C., Nicolls, M., et al. (2012). Comparing VHF coherent scatter from the radar aurora with incoherent scatter and all-sky auroral imagery. *Journal of Geophysical Research*, *117*(A10), A10313. <https://doi.org/10.1029/2012JA018010>
- Imajo, S., Miyoshi, Y., Kazama, Y., Asamura, K., Shinohara, I., Shiohara, K., et al. (2021). Active auroral arc powered by accelerated electrons from very high altitudes. *Scientific Reports*, *11*(1), 1610. <https://doi.org/10.1038/s41598-020-79665-5>
- Ivarsen, M. F., Gilles, D. M., Huyghebaert, D. R., St-Maurice, J. P., Lozinsky, A., Galeschuk, D., & Hussey, G. (2024). Turbulence embedded into the ionosphere by electromagnetic waves. *JGR: Space Physics*, *128*(1), e2023JA031585. <https://doi.org/10.1029/2022ja031050>
- Ivarsen, M. F., Lozinsky, A., St-Maurice, J.-P., Spicher, A., Huyghebaert, D., Hussey, G. C., et al. (2023). The distribution of small-scale irregularities in the E-region, and its tendency to match the spectrum of field-aligned current structures in the F-region. *Journal of Geophysical Research: Space Physics*, *128*(5), e2022JA031233. <https://doi.org/10.1029/2022JA031233>
- Ivarsen, M. F., St-Maurice, J.-P., Hussey, G., Spicher, A., Jin, Y., Lozinsky, A., et al. (2023). Measuring small-scale plasma irregularities in the high-latitude E- and F-regions simultaneously. *Scientific Reports*, *13*(1), 11579. <https://doi.org/10.1038/s41598-023-38777-4>
- Ivarsen, M. F., St-Maurice, J.-P., Hussey, G. C., Galeschuk, D., Lozinsky, A., Pitzel, B., & McWilliams, K. A. (2023). An algorithm to separate ionospheric turbulence radar echoes from those of meteor trails in large data sets. *Journal of Geophysical Research: Space Physics*, *128*(1), e2022JA031050. <https://doi.org/10.1029/2022JA031050>
- Karlsson, T., Andersson, L., Gillies, D. M., Lynch, K., Marghitu, O., Partamies, N., et al. (2020). Quiet, discrete auroral arcs—Observations. *Space Science Reviews*, *216*(1), 16. <https://doi.org/10.1007/s11214-020-0641-7>
- Kasahara, S., Miyoshi, Y., Yokota, S., Mitani, T., Kasahara, Y., Matsuda, S., et al. (2018). Pulsating aurora from electron scattering by chorus waves. *Nature*, *554*(7692), 337–340. <https://doi.org/10.1038/nature25505>
- Keiling, A., Thaller, S., Wygant, J., & Dombeck, J. (2019). Assessing the global Alfvén wave power flow into and out of the auroral acceleration region during geomagnetic storms. *Science Advances*, *5*(6), eaav8411. <https://doi.org/10.1126/sciadv.aav8411>
- Kikuchi, S., Kobayashi, D., Yasuda, H., Ueno, H., & Thorpe, L. (2016). *Canon knowledge base—White paper: Advances in CMOS image sensors and associated processing*. Canon. Retrieved from <https://support.usa.canon.com/kb/index?page=content&id=ART170243>
- Kintner, P. M., Ledvina, B. M., & de Paula, E. R. (2007). GPS and ionospheric scintillations. *Space Weather*, *5*(9), S09003. <https://doi.org/10.1029/2006SW000260>
- Liu, J., Wang, W., Burns, A., Oppenheim, M., & Dimant, Y. (2018). Faster traveling atmosphere disturbances caused by polar ionosphere turbulence heating. *Journal of Geophysical Research: Space Physics*, *123*(3), 2181–2191. <https://doi.org/10.1002/2017JA024746>
- Lozinsky, A., Hussey, G., McWilliams, K., Huyghebaert, D., & Galeschuk, D. (2022). ICEBEAR-3D: A low elevation imaging radar using a non-uniform coplanar receiver array for E region observations. *Radio Science*, *57*(3), e2021RS007358. <https://doi.org/10.1029/2021RS007358>
- Lysak, R., & Dum, C. T. (1983). Dynamics of magnetosphere-ionosphere coupling including turbulent transport. *Journal of Geophysical Research*, *88*(A1), 365–380. <https://doi.org/10.1029/JA088iA01p00365>
- Lysak, R., Echim, M., Karlsson, T., Marghitu, O., Rankin, R., Song, Y., & Watanabe, T.-H. (2020). Quiet, discrete auroral arcs: Acceleration mechanisms. *Space Science Reviews*, *216*(5), 92. <https://doi.org/10.1007/s11214-020-00715-5>
- Lysak, R., & Song, Y. (2003). Kinetic theory of the Alfvén wave acceleration of auroral electrons. *Journal of Geophysical Research*, *108*(A4), 8005. <https://doi.org/10.1029/2002JA009406>
- Mallinckrodt, A. J., & Carlson, C. W. (1978). Relations between transverse electric fields and field-aligned currents. *Journal of Geophysical Research*, *83*(A4), 1426–1432. <https://doi.org/10.1029/JA083iA04p01426>
- Marklund, G. (2009). Electric fields and plasma processes in the auroral downward current region, below, within, and above the acceleration region. *Space Science Reviews*, *142*(1), 1–21. <https://doi.org/10.1007/s11214-008-9373-9>
- Marklund, G., Johansson, T., Lileo, S., & Karlsson, T. (2007). Cluster observations of an auroral potential and associated field-aligned current reconfiguration during thinning of the plasma sheet boundary layer. *Journal of Geophysical Research*, *112*(A1), A05204. <https://doi.org/10.1029/2006JA011804>

- Mozer, F. S., Carlson, C. W., Hudson, M. K., Torbert, R. B., Parady, B., Yatteau, J., & Kelley, M. C. (1977). Observations of paired electrostatic shocks in the polar magnetosphere. *Physical Review Letters*, *38*(6), 292–295. <https://doi.org/10.1103/PhysRevLett.38.292>
- Noël, J.-M. A., St. Maurice, J.-P., & Blelly, P.-L. (2000). Nonlinear model of short-scale electrodynamic in the auroral ionosphere. *Annales Geophysicae*, *18*(9), 1128–1144. <https://doi.org/10.1007/s00585-000-1128-1>
- Noël, J.-M. A., St. Maurice, J.-P., & Blelly, P.-L. (2005). The effect of E-region wave heating on electrodynamic structures. *Annales Geophysicae*, *23*(6), 2081–2094. <https://doi.org/10.5194/angeo-23-2081-2005>
- Oppenheim, M. (1997). Evidence and effects of a wave-driven nonlinear current in the equatorial electrojet. *Annales Geophysicae*, *15*(7), 899–907. <https://doi.org/10.1007/s00585-997-0899-z>
- Palmroth, M., Grandin, M., Sarris, T., Doornbos, E., Tourgaidis, S., Aikio, A., et al. (2021). Lower-thermosphere–ionosphere (LTI) quantities: Current status of measuring techniques and models. *Annales Geophysicae*, *39*(1), 189–237. <https://doi.org/10.5194/angeo-39-189-2021>
- RGB, T. (2023). UCalgary space remote sensing group data landing page—UCalgary SRS data documentation [Dataset]. *University of Calgary*. <https://doi.org/10.11575/4P8E-1K65>
- Roth, M., Evans, D. S., & Lemaire, J. (1993). Theoretical structure of a magnetospheric plasma boundary: Application to the formation of discrete auroral arcs. *Journal of Geophysical Research*, *98*(A7), 11411–11423. <https://doi.org/10.1029/93JA00156>
- Schlegel, K., & St.-Maurice, J. P. (1981). Anomalous heating of the polar E region by unstable plasma waves 1. Observations. *Journal of Geophysical Research*, *86*(A3), 1447–1452. <https://doi.org/10.1029/JA086iA03p01447>
- Semeter, J., Mrak, S., Hirsch, M., Swoboda, J., Akbari, H., Starr, G., et al. (2017). GPS signal corruption by the discrete aurora: Precise measurements from the Mahali experiment. *Geophysical Research Letters*, *44*(19), 9539–9546. <https://doi.org/10.1002/2017GL073570>
- Senior, C., Robinson, R. M., & Potemra, T. A. (1982). Relationship between field-aligned currents, diffuse auroral precipitation and the westward electrojet in the early morning sector. *Journal of Geophysical Research*, *87*(A12), 10469–10477. <https://doi.org/10.1029/JA087iA12p10469>
- Seyler, C. E., Clark, A. E., Bonnell, J., & Wahlund, J.-E. (1998). Electrostatic broadband ELF wave emission by Alfvén wave breaking. *Journal of Geophysical Research*, *103*(A4), 7027–7041. <https://doi.org/10.1029/97JA02297>
- Siscoe, G. L., Erickson, G. M., Sonnerup, B. U. O., Maynard, N. C., Schoendorf, J. A., Siebert, K. D., et al. (2002). Hill model of transpolar potential saturation: Comparisons with MHD simulations. *Journal of Geophysical Research*, *107*(A6), SMP8-1–SMP8-8. <https://doi.org/10.1029/2001JA000109>
- St-Maurice, J.-P., & Goodwin, L. (2021). Revisiting the behavior of the E-region electron temperature during strong electric field events at high latitudes. *Journal of Geophysical Research: Space Physics*, *126*(2), 2020JA028288. <https://doi.org/10.1029/2020JA028288>
- St-Maurice, J.-P., Huyghebaert, D., Ivarsen, M. F., & Hussey, G. C. (2023). Narrow Width Farley-Buneman spectra above 100 km altitude. *Journal of Geophysical Research: Space Physics*, *128*(10), e2022JA031191. <https://doi.org/10.1029/2022JA031191>
- St-Maurice, J. P., Kofman, W., & James, D. (1996). In situ generation of intense parallel electric fields in the lower ionosphere. *Journal of Geophysical Research*, *101*(A1), 335–356. <https://doi.org/10.1029/95JA02586>
- Thayer, J. P. (1998). Height-resolved Joule heating rates in the high-latitude E region and the influence of neutral winds. *Journal of Geophysical Research*, *103*(A1), 471–487. <https://doi.org/10.1029/97JA02536>
- Themens, D. R., Jayachandran, P., McCaffrey, A. M., Reid, B., & Varney, R. H. (2019). A bottomside parameterization for the empirical Canadian high arctic ionospheric model. *Radio Science*, *54*(5), 397–414. <https://doi.org/10.1029/2018RS006748>
- Themens, D. R., Jayachandran, P. T., Bilitza, D., Erickson, P. J., Häggström, I., Lyashenko, M. V., et al. (2018). Topside electron density representations for middle and high latitudes: A topside parameterization for E-CHAIM based on the NeQuick. *Journal of Geophysical Research: Space Physics*, *123*(2), 1603–1617. <https://doi.org/10.1002/2017JA024817>
- Themens, D. R., Jayachandran, P. T., Galkin, I., & Hall, C. (2017). The Empirical Canadian high Arctic ionospheric model (E-CHAIM): NmF2 and hmF2. *Journal of Geophysical Research: Space Physics*, *122*(8), 9015–9031. <https://doi.org/10.1002/2017JA024398>
- Watermann, J. (1990). Refraction of 50-MHz radar waves in a realistic ionospheric model. *Radio Science*, *25*(5), 805–812. <https://doi.org/10.1029/RS025i005p0805>
- Watson, C., Themens, D. R., & Jayachandran, P. T. (2021). Development and Validation of precipitation enhanced Densities for the empirical Canadian high Arctic ionospheric model. *Space Weather*, *19*(10), e2021SW002779. <https://doi.org/10.1029/2021SW002779>
- Wiltberger, M., Merkin, V., Zhang, B., Toffoletto, F., Oppenheim, M., Wang, W., et al. (2017). Effects of electrojet turbulence on a magnetosphere-ionosphere simulation of a geomagnetic storm. *Journal of Geophysical Research: Space Physics*, *122*(5), 5008–5027. <https://doi.org/10.1002/2016JA023700>
- Winglee, R. M., Papitashvili, V. O., & Weimar, D. R. (1997). Comparison of the high-latitude ionospheric electrodynamic inferred from global simulations and semiempirical models for the January 1992 GEM campaign. *Journal of Geophysical Research*, *102*(A12), 26961–26977. <https://doi.org/10.1029/97JA02461>
- Yeh, K. C., & Liu, C.-H. (1982). Radio wave scintillations in the ionosphere. *IEEE Proceedings*, *70*(4), 324–360. <https://doi.org/10.1109/proc.1982.12313>